Rose flower-shaped CuS nanostructures: a study on different properties and photocatalytic performance

Vishal Dhiman[1] · Manmeet Kaur[1] · Dixit Prasher[1,2] · Deepesh Bhardwaj[3] · Kushvinder Kumar[4] · Suresh Kumar[1]

Abstract

Photocatalysts have gained much attention because of the water pollution instigated by the rapid usage of organic dyes for industrial needs. The degradation of these dyes using photocatalysts under natural light is an economical and popular method for water treatment. There is a need to synthesize photocatalytic materials which can generate reactive oxygen species under natural light. Hence, keeping in mind the above point, rose flower-shaped CuS nanostructures have been synthesized first time by solvothermal technique by varying reaction duration. The self-assembled powder of CuS nanostructures is characterized using XRD, FE-SEM, TEM, DLS, EDS, XPS, Raman, FT-IR, and UV–visible spectroscopy. The XRD and TEM analyses confirmed the formation of a polycrystalline hexagonal structure with prominent diffraction peaks. FE-SEM study shows the formation of uniformly self-assembled rose flower-shaped nanostructures of size 2–3 μm composed of densely packed nanoparticles. XPS study shows the presence of Cu(II) and Cu(I) states of copper in the synthesized batch and stoichiometric composition Cu:S is found to be 60:40 *at.%*. The optical studies showed broad absorption spectra of CuS nanostructures in about 300–800 nm wavelength range. Besides, this work studies the degradation activity of methylene blue and crystal violet organic dyes under natural sunlight conditions without the presence of any additive agent.

Graphical abstract
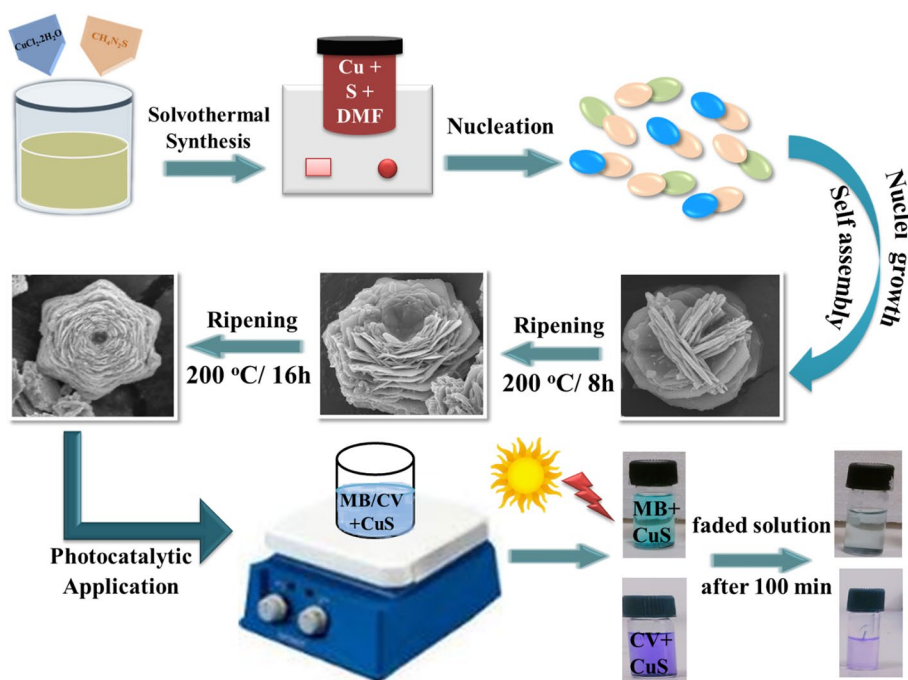
Extended author information available on the last page of the article

1 Introduction

Rapid industrial growth and extensive use of chemicals for industrial purposes have severely contaminated the environment. Different dyes used in the textile and other industries heavily polluted the water bodies and soil at large. Organic dyes such as methylene blue, methyl orange, Congo red, and crystal violet are toxic in nature and pose serious challenges and threats to human health and the environment [1]. To settle down, the challenge of the increasing use of dyes in different industries is a very big challenge for all research communities. Among different organic dyes, methylene blue (MB) is a toxic, mutagenic, and non-biodegradable cationic dye, commonly used in textile, pharmaceutics, and aquaculture as a fungicide and antidotes, that can seriously threaten the ecology [2]. Likewise, crystal violet (CV) is a cationic triphenylmethane dye, a highly demanded industrial raw material that is used in textile materials (such as cotton and silk), in ternary materials (such as leather and animal skin), and as an external disinfectant due to its harmful effect on cells [3]. In recent years, many attempts have been made to minimize the pollution arising from the use of these dyes in the industry. One of the big contributions to minimizing this serious problem is the use of solar energy to degrade the dyes using suitable photocatalysts [4]. Further, the generation of hydroxyl radicals (OH·) is an important factor for the photocatalytic degradation of dyestuffs. Narrow bandgap and single-phase materials such as TiO_2-based, graphitic-C_3N_4, Ag_3PO_4, and metal oxide-based materials have been developed to enhance photocatalytic performance [5, 6]. Another side of photodegradation is the photo-Fenton reactions to produce OH· under acidic conditions i.e., a pH-dependent procedure. However, there are complications in maintaining and proceeding under narrow *p*H values for dye degradation. In addition, many common photocatalytic materials like TiO_2 having lattice defects hinder photocatalytic activity [7, 8]. Consequently, there is a need to explore catalyst materials that work beyond such limitations. The photocatalytic performance of catalysts in the degradation process depends on different factors such as the surface-to-volume ratio, optical bandgap, and excited state energy [9]. The chalcogenide-based catalysts when exposed to incident photons produced charge carriers having high redox potential [10]. The charge carriers so produced generate primary reactive oxygen species (ROS) in the reaction with oxygen (O_2) and water (H_2O) which further leads to breaks the dyestuffs and other organic pollutants that are present in the environment. The copper-based chalcogenides are earth-abundant and non-toxic materials that show excellent potential in the photocatalysis process.

Copper sulfide (CuS), a class of copper-based chalcogenides, is a *p*-type semiconductor that is free from any toxic composition, has a narrow band gap and higher reactivity than TiO_2, making it a promising material that superbly responds in the visible and near-infrared light region [11, 12]. CuS material series include various phases such as copper-rich chalcocite (Cu_2S), copper-deficient villamaninite (CuS_2), covellite (CuS), yarrowite ($Cu_{1.12}S$), spionkopite ($Cu_{1.39}S$), geerite ($Cu_{1.6}S$), anilite ($Cu_{1.75}S$), digenite ($Cu_{1.8}S$), and djurleite ($Cu_{1.96}S$) [13–15]. In general, different phases of CuS series can be synthesized by controlling the particle size and morphology which is further attributed to tuning the physical, chemical, optical, and electronic properties without changing chemical composition [13–16]. Many researchers have reported different morphology of the CuS materials such as flower and branch structures, hexagonal plates, dandelion tubes, and spherical-shaped particles under the effect of reaction time, temperature, solvent, composition, etc., [4, 7, 8, 14–20]. Different methods are employed to synthesize CuS materials such as hydrothermal, solvothermal, chemical vapor deposition, solid-state combustion, coprecipitation, and sol–gel [17–19]. Among these methods, the hydro/solvothermal method has the advantage of tuning material surfaces into different morphology simply by controlling the reaction conditions [20, 21]. In a recent work, unusual novel morphologies such as the irregular, regular, trigonal, hexagonal leaf, and snowflakes dendrites were synthesized using a hydrothermal route by varying reaction time from 8 to 24 h and temperatures (60–200 °C) [20]. This work is an attempt to explore possibilities of dye degradation beyond the limitations of the photo-Fenton reaction and the lattice defects. Metal sulfides such as CdS, ZnS, MoS_2, SnS_2, and Bi_2S_3 have played an extensive role in photocatalytic degradation activities [22]. Copper-based chalcogenides exhibit unique physical, chemical, optical, and electronic properties and possess numerous applications in photocatalysis. Herein, the degradation of MB and CV dyes has been achieved using CuS nanostructures and the reactive oxygen sites are attained without adding additive agents like H_2O_2 [23]. The present work focuses on the synthesis of CuS nanostructures from the non-aqueous N,N-dimethylformamide (DMF) solvent through the solvothermal technique by changing the reaction time. The structural, morphological, and optical properties of synthesized nanostructures have been analyzed using different characterization techniques. In addition, the ability of the synthesized samples

to photocatalyze the degradation of MB and CV dyes under the influence of natural sunlight has been analyzed.

2 Experimental details

2.1 Materials

In the present work, analytical grade chemicals, i.e., copper (II) chloride ($CuCl_2.2H_2O$), thiourea (CH_4N_2S), and N,N-dimethyl formamide (DMF) were purchased from chemical drug house (CDH), India and were used without further purification.

2.2 Solvothermal synthesis of CuS nanostructures

To synthesize CuS nanostructures, precursor salts of copper chloride (0.1 M), and thiourea (0.2 M) were appropriated in 50 mL DMF solution and stirred continuously for 90 min at room temperature to achieve a clear and homogeneous solution. The final solution was poured into a 75 mL Teflon liner-covered stainless-steel autoclave which was further kept in a solvothermal reactor. Now, to obtain definite morphology and structure of CuS material, the reactor was maintained at a fixed temperature of 200 °C, while the reaction time was varied for 8 h and 16 h. After the complete reaction process, a black-colored product was obtained which was further processed for aging and kept for another 16 h. Thereafter, the aged black-colored material was centrifuged using REMI CPR-30 to separate the desired product from impurities or waste. Finally, the obtained samples were dried at 200 °C in a hot air vacuum oven for 2 h and then stored in a vacuum desiccator till they were used for different characterizations.

2.3 Characterization techniques

X-ray diffraction (XRD) patterns of CuS nanostructures, that are synthesized in the powder form, were obtained using XRD: PANalytical X'Pert Pro having Cu-Kα radiation ($\lambda = 1.5406$ Å) operated at 45 kV/40 mA at a scanning rate of 0.05 s^{-1}. Field emission scanning electron micrographs (FE-SEM) were taken using SEM: Hitachi S-4800 coupled with an energy-dispersive X-ray spectroscope (EDS: Bruker). To prevent the charging of the sample in FE-SEM characterization, they were sputter coated with gold (~ 1.5 to 3 nm) after being mounted on aluminum stubs using double-sided carbon tape. To get the direct imaging of the CuS sample, transmission electron microscopy (TEM: JEOL-JEM 2100 plus) was performed at an accelerating voltage of 200 kV. A sample for TEM characterization was prepared by dispersing the CuS nanostructures in ethanol solution and sonicating for 10 min. Subsequently, a drop of the dispersion (20 μL) was deposited on a carbon-coated Cu-grid and left to air dry. The dynamic light scattering (DLS) measurements were conducted on the CuS nanostructures at 25 °C using a particle size analyzer (Anton Paar: Litesizer). The suspensions for DLS measurements were prepared by dissolving 1 mg of each CuS sample in the double-distilled water and sonicating them for 20 min to deagglomerate the particles. All powder samples were characterized by an X-ray photoelectron spectrometer (XPS: PHI 5000 VersaProbe III) equipped with an Al-Kα monochromatic X-ray source. Raman and FT-IR spectra were obtained using WITec: Alpha300R and Shimadzu: 00293 spectrometers, respectively, to examine the compositions of the synthesized samples. The KBr pellet technique was adopted to prepare samples for FT-IR measurements where CuS nanostructures were mixed with KBr salt and hydraulically pressed into pellets. UV–visible spectrophotometer (Perkin Elmer: Lambda-750) was used to get information about absorption in the wavelength range of 300–800 nm. The liquid samples for UV–visible measurement were prepared by dispersing a small amount of CuS nanostructures in ethanol.

2.4 Photocatalytic degradation of MB and CV dyes

The photocatalytic performance of the synthesized material in the presence of natural sunlight was examined over the solutions of the selected dyes i.e., MB and CV that were prepared using double-distilled water. Typically, 0.5 mg of CuS catalysts, which are synthesized for the reaction duration of 8 h and 16 h, were mixed with the 25 mL solutions of each selected dye, and their photocatalytic behavior was tested. To maintain the equilibrium, the solutions were kept in the dark chamber under a constant stirring rate for 30 min intended to adsorb the dye molecules on the surface of the CuS catalyst. Thereafter, the solutions were transferred to equally sized borosil glass tubes and kept under a natural sunlight environment for an exposure time of 100 min. During the photocatalytic experiment, a 5 mL solution of the degraded samples from each reaction tube was collected at every 20 min sequentially. The catalyst was separated from these solutions by centrifugation at 2000 rpm, and filtering through a 0.45 μm membrane. The concentration of dye samples after degradation activity was finally analyzed using a UV–visible absorbance spectrophotometer, wherein the absorbance was recorded over the wavelength range of 300–800 nm.

3 Results and discussion

3.1 Structural studies

The typical XRD patterns, Fig. 1a, b, reveal the phase and purity of the synthesized CuS nanostructures at reaction
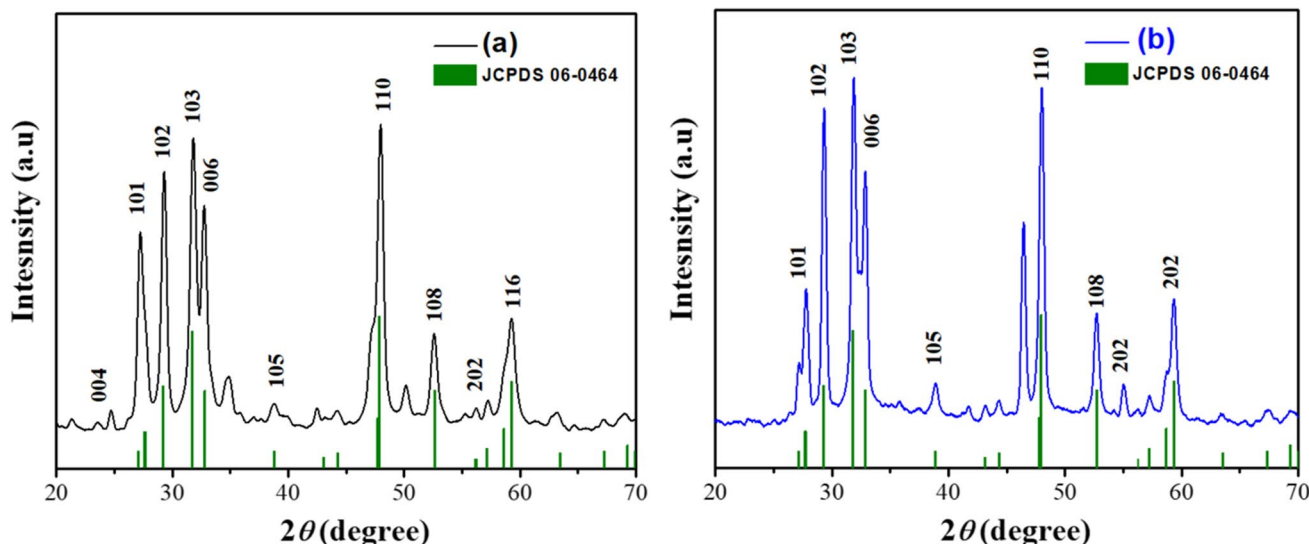
Fig. 1 XRD patterns of CuS nanostructures at the reaction time **a** 8 h and **b** 16 h

Table 1 Structural parameters, i.e., average crystallite size, lattice constants, dislocation density, and microstrain calculated for the synthesized CuS nanostructures

Sample	Crystallite size D_{xrd} (nm)	Lattice constants (Å)		Dislocation density (nm)$^{-2}$	Microstrain
		a	c		
CuS (8 h)	14.13	3.61	15.67	5.01×10^{-3}	8.02×10^{-2}
CuS (16 h)	17.25	3.63	15.69	4.06×10^{-3}	5.53×10^{-2}

times of 8 h and 16 h. The XRD spectra displayed diffraction peaks at different angles, $2\theta = 22.44°$, 27.6°, 29.2°, 31.8°, 32.7°, 38.12°, 48.02°, 52.5°, 56.21°, and 59.2° which are corresponding to the Miller planes as assigned to (*004*), (*101*), (*102*), (*103*), (*006*), (*105*), (*110*), (*108*), (*202*), and (*116*), respectively [24–26]. These diffraction peaks are indexed to the hexagonal phase associated with the geerite structure of CuS (JCPDS Card File No. 06–0464) [27]. Moreover, the absence of any noticeable peaks in the XRD spectra strengthens the pure phase formation of CuS nanostructure with a polycrystalline nature. The low-intensity peaks at $2\theta = 34.8°$, 42.4°, 44.1°, 50.1°, 63.1°, and 67° for sample synthesized at 8 h probably due to the under-developed phases of CuS whereas with longer reaction time the formation of nanostructures completed. The average crystallite size (D_{xrd}) of the synthesized samples (Table 1) was estimated using Debye–Scherrer's formula [28]:

$$D_{xrd} = \frac{k\lambda}{\beta\cos\theta} \tag{1}$$

where k, λ, β, and θ are the shape factor, the wavelength of X-ray used, full-width half maxima of the featured peak, and Bragg's angle, respectively. The lattice constants (a and c) associated to the hexagonal structure were calculated using [29]

$$\frac{1}{d^2} = \frac{4}{3}\left(\frac{h^2 + hk + k^2}{a^2}\right) + \frac{l^2}{c^2} \tag{2}$$

The terms used here have their specific meaning, (*hkl*) denotes Miller indices of the defined planes, and d stands for inter-planar distance. The calculated values of lattice constants (Table 1) and $c/a = 4.34$ for CuS nanostructures are found close to the reported [19]. The crystallites size and lattice constants were increased, while dislocation density and microstrain decreased with the increasing reaction time which is probability due to the complete growth of the nanostructures [30, 31].

3.2 Morphological studies

The effect of the reaction time on the morphology of the CuS nanostructures is evinced from the field emission scanning electron microscopic (FE-SEM) images (Fig. 2a–d) that displayed self-assembled rose flower-shaped morphology for the fully developed CuS nanostructures. It also reveals that the rose-like regular assemblies are formed as a result of the symmetrical combination of nanoflakes. In addition, with higher reaction time, fully developed hexagonal structures (insert Fig. 2c) are also found with round-shaped flowers without any noticeable change in the assembly of the nanostructures. This type of morphology in synthesized CuS nanostructures may be attributed to the complex formation

Fig. 2 FE-SEM images for CuS nanostructures with reaction times of 8 h (**a**, **b**) and 16 h (**c**, **d**) at two different magnifications, i.e., 20 μm and 10 μm, respectively
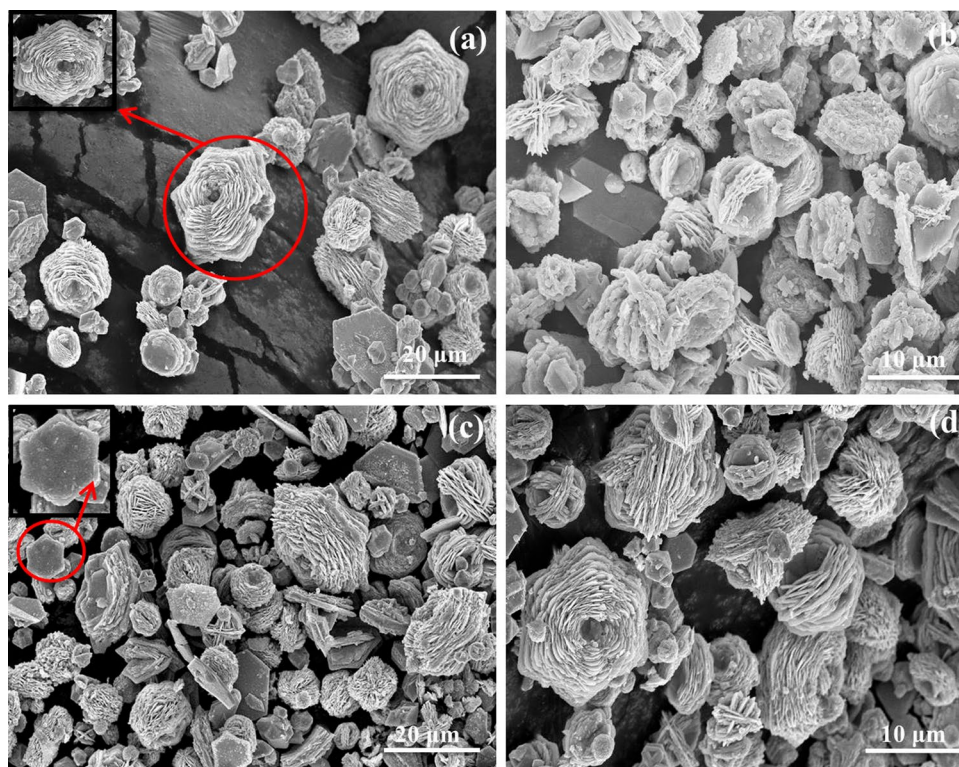
between DMF and Cu-ions [32, 33]. Further, to minimize the surface energy these nanoflakes are self-assembled and grown up in hexagonal rose flower-like structures due to the privileged Ostwald ripening [34, 35]. Many researchers have reported spherical, marigold, doughnut-shaped structures for CuS material using the solvothermal/hydrothermal technique [36]. The average size of each such flower is observed to be 5–10 μm; however, hexagonal sheet has a size range between 2 and 5 μm. It is clear from the observed morphology that high reaction time offers an environment for the nanoflakes to be assembled in rose-like regular structures with large volumes. Thus, it can be concluded that substantial changes in the morphology of the CuS nanostructures are promoted by the reaction time in the solvothermal technique.

Figure 3a–c displays the transmission electron microscopic (TEM) micrographs of synthesized CuS nanostructures for a reaction duration of 16 h. Almost equal-sized nanoparticles are found in a dense morphology whereas a few individual nanoflakes are also found to be scattered in the background. Figure 3b reveals the individual image of a flower-shaped structure which is in good contrast with FE-SEM images. In the SAED pattern (Fig. 3d), the electron diffraction patterns in the form of concentric rings, at $(1\bar{1}01)$, $(1\bar{1}03)$, $(1\bar{1}05)$, $(01\bar{1}0)$, $(1\bar{1}08)$, and $\left(1\bar{2}12\right)$ correspond to the hexagonal structure of CuS and are further supported by the reported literature [37, 38]. The detected central bright spot along with concentric rings (Fig. 3d) is evident in the extent of high polycrystallinity in the synthesized material which is already confirmed by the XRD study.

DLS technique based on the Brownian movement is used to estimate the zeta potential (i.e., charge on the surface of nanoparticles) and size of hydro-dynamically suspended particles. The high value of zeta potential tends to hinder the coagulation of particles which further supports electrically more stable particles. Here, the zeta potential values for CuS nanostructures synthesized at reaction times of 8 h and 16 h were measured to be – 19.79 mV and – 9.92 mV, respectively, Fig. 4a and c. Its negative value indicates the formation of hydroxyl groups on the surface of nanoparticles upon dispersion in distilled water. The mean diameter of the CuS nanostructures, synthesized at reaction times of 8 h and 16 h, in the aqueous suspension, has been determined to be 23.48 ± 8 nm and 32.47 ± 10 nm, respectively, Fig. 4b and d. The hydrodynamic size observed from DLS measurement, which is somewhat larger than that obtained from XRD analysis, may be attributed to the contribution of the electrical double layer around the nanoparticles [39].

3.3 Compositional studies

Energy-dispersive spectroscopy (EDS) was performed to confirm the stoichiometric proportion of the prepared CuS nanostructures as shown in Fig. 5a and b. The peaks obtained in EDS spectra confirm the presence of Cu and S elements in synthesized samples. Further, the absence of any

Fig. 3 TEM images for CuS nanostructures synthesized at a reaction time of 16 h at different resolutions **a** 500 nm, **b** 50 nm, **c** 100 nm and **d** SAED pattern
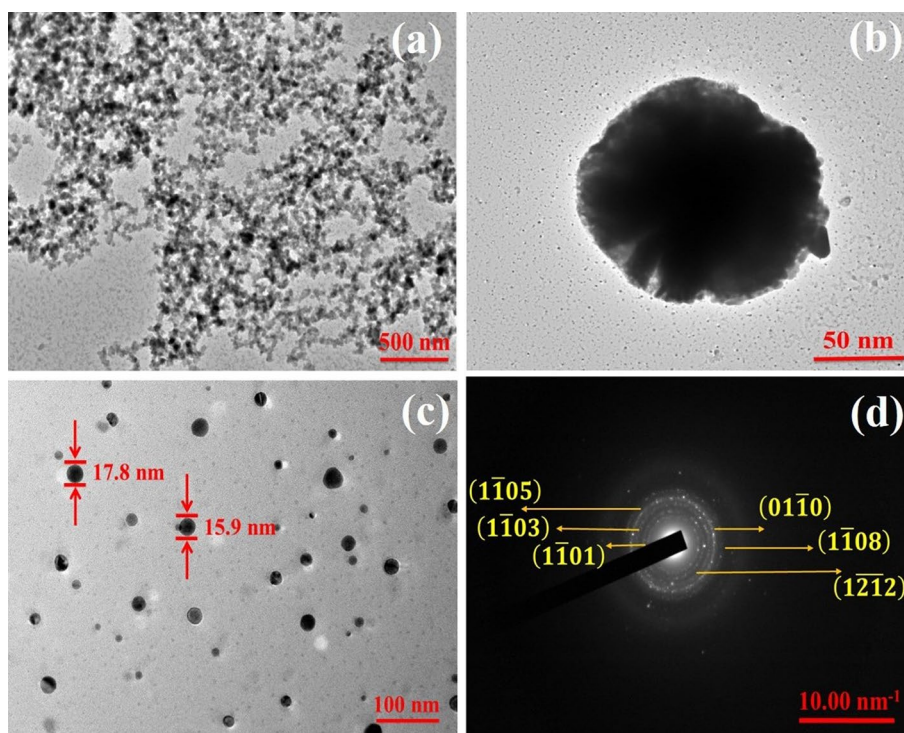
other elemental peaks depicted that the synthesized material is free from elemental impurities. It is analyzed that the stoichiometry of the synthesized CuS nanostructures is independent of the reaction time. The stoichiometric ratio (*at. %*) for Cu:S in both samples is found to be 60:40, i.e., 1.5:1 which also confirms the formation of the geerite ($Cu_{1.5}S$) phase of copper sulfide.

3.4 XPS studies

To understand the composition, oxidation state, and surface chemistry of Cu and S elements present in the synthesized CuS nanostructures the X-ray photoelectron spectroscopy (XPS) measurements were carried out and shown in Figs. 6 and 7. The survey scans (Figs. 6a and 7a) show the full XPS spectra of CuS nanostructures that confirm the existence of Cu and S elements by their characteristic peaks. Besides these peaks, a carbon (C) peak is observed that may be from the reference material used in the characterization or the chemisorption of functional groups on the surface of CuS nanostructures [40]. Moreover, the oxygen peak is also there because of the moisture content on the CuS surface from the surrounding atmosphere. The absence of impurities such as nitrogen, chlorine, and sodium, in the XPS survey scan shows the purity of the synthesized CuS nanostructures. In the narrow scan spectra for the Cu element (Figs. 6b and 7b), the peak obtained at 931.8 and 951.5 eV belong to Cu^{1+} binding energies of Cu $2p_{3/2}$ and Cu $2p_{1/2}$ of monovalent Cu(I), respectively [41]. Further,

the Cu^{1+} oxidation state is confirmed by the establishment of a spin–orbit separation of 19.7 eV. In addition, a peak at ~945 eV (Figure b) corresponds to the existence of the paramagnetic chemical state of Cu^{2+} [40, 41]. The presence of dual oxidation states (Cu^{1+} and Cu^{2+}) of copper in CuS structures was also reported in the literature [40, 41]. In the same manner, the narrow scan spectrum of S (Figs. 6c and 7c) showed two peaks between 162 and 164 eV corresponding to the spin–orbit split of S $2p_{1/2}$ and $2p_{3/2}$ which confirms the S^{2-} oxidation state. The peaks close to 164 eV and 169 eV are related to the S^{2-} (metal-S) bond and satellite peak, respectively [42, 43]. From these peaks, it is found that the peak observed toward the higher binding energy side (i.e., toward 164 eV) is related to mono-sulfide bonded with Cu^{2+} centers, whereas the peak observed toward the lower binding energy side (i.e., toward 162 eV) was attributed to the di-sulfides. Further, it has been reported that both monosulfide and di-sulfide atoms are responsible for S 2p peak splitting in the hexagonal CuS. The chemical composition and binding energies attained by XPS analysis are observed to be in accordance with the previous reports [40, 42, 43]. Therefore, the observed XPS peaks are well correlated with the valency distribution of copper and sulfur in the hexagonal structure of CuS.

3.5 Raman and FT-IR studies

As Cu and S have very close diffraction angles in order to confirm the phase formation in synthesized CuS material,
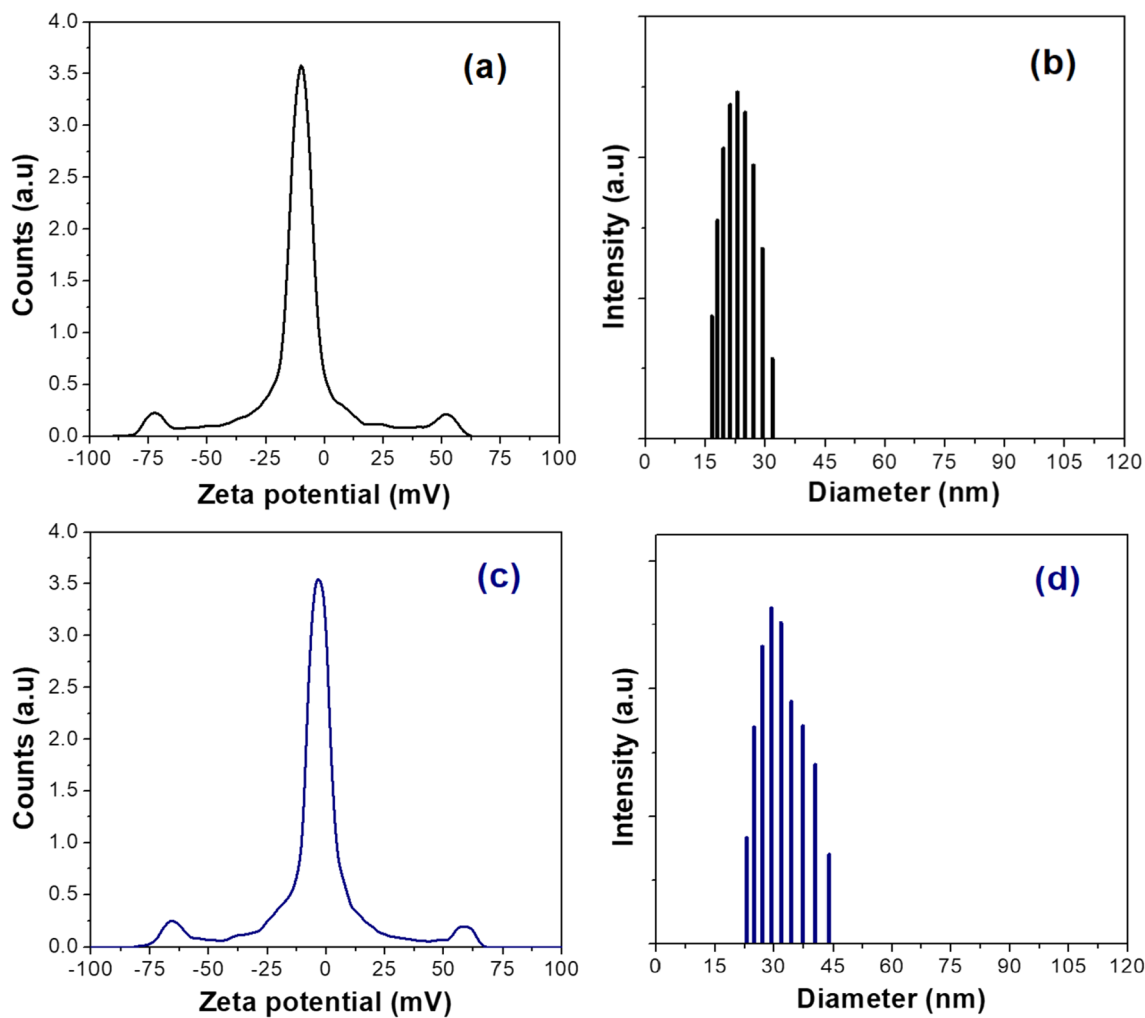
Fig. 4 Zeta potential and particle size distribution of the synthesized CuS nanostructures synthesized at a reaction time of 8 h (**a**, **b**) and 16 h (**c**, **d**), respectively
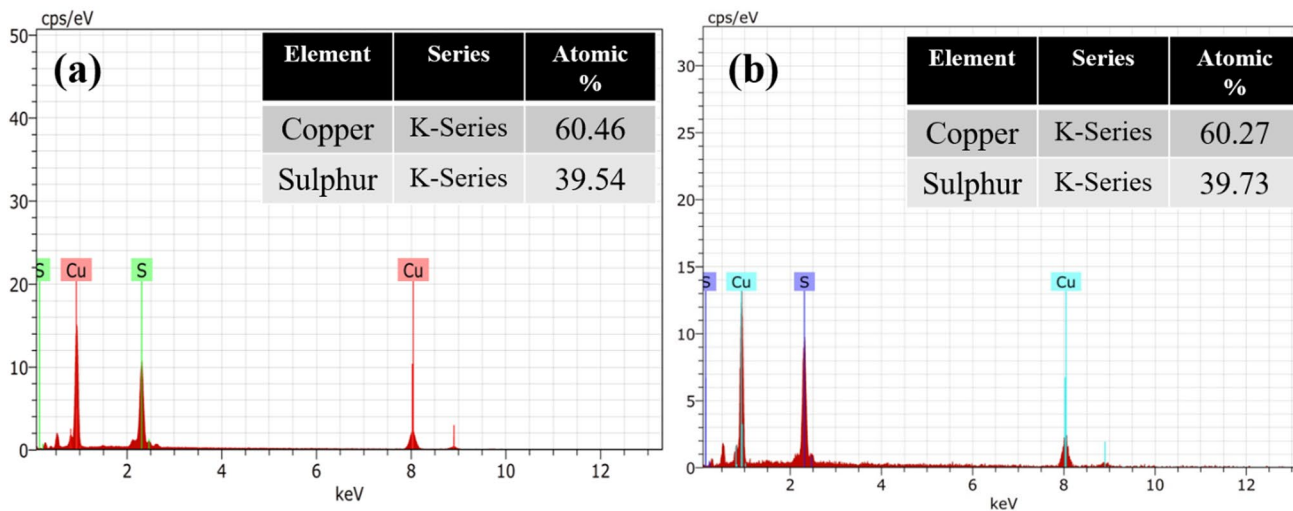
Fig. 5 EDS spectra for CuS nanostructures synthesized at a reaction time of **a** 8 h and **b** 16 h
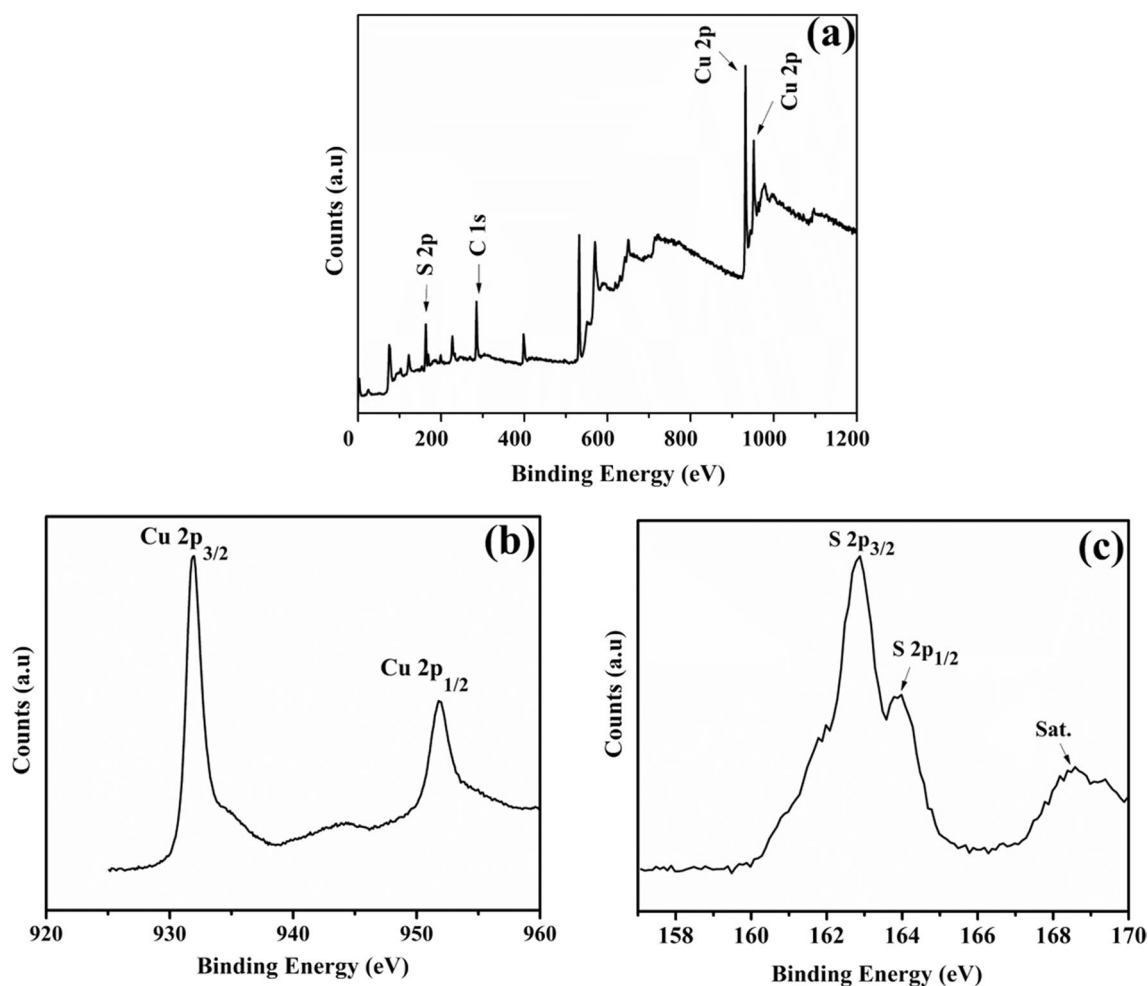
Fig. 6 XPS spectra for **a** survey scan, **b** copper (Cu), **c** sulfur (S) for CuS nanostructures synthesized at a reaction time of 8 h

Raman spectroscopy was done and Raman spectra for both samples are represented in Figs. 8a and b. Both spectra reveal a weak peak at about 266 cm^{-1} and a pronounced peak at ~473 cm^{-1} which are assigned to the Cu–S bond vibrations and S–S vibrational (stretching) mode of S$_2$ ion at 4e sites, respectively. It represents the good crystallinity of the synthesized nanostructures [44, 45]. The peaks belonging to Cu$_2$O (218/523/623 cm^{-1}) and CuO (298/347/591 cm^{-1}) are not found in these spectra which confirms the existence of pure and crystalline CuS material [46].

To check the presence of different functional groups in the chemically synthesized samples, Fourier transform infrared (FT-IR) spectra were recorded, Fig. 9a and b. A broad absorbance band between ~3400 and 3300 cm^{-1} is shared by the O–H stretching vibration of water molecules, which may be due to the moisture content in the air, and N–H stretching vibrations that are obtained because of the use of H$_2$N–C–NH$_2$ as a source of sulfur during the synthesis. A strong peak obtained at 2972 cm^{-1} is assigned to C–H stretching. Different weak peaks at 2504 cm^{-1},

2242 cm^{-1}, 2062 cm^{-1}, 1998 cm^{-1}, and 1959 cm^{-1} belong to O–H, –C–C–, N=C=S bonding and aromatic overtones [47–50]. The peak obtained at 1689.64 cm^{-1} corresponds to δN–H bending deformity. Similarly, the peaks obtained at 1411 cm^{-1} and 1380 cm^{-1} are because of S=O stretching [48]. The strong peaks at 1107 cm^{-1}, 1056 cm^{-1}, and 833 cm^{-1} are claimed because of asymmetric stretching of the carbonyl (C=O) group, C–O bonding, and C–halogen bonding, respectively. The peaks that occurred at 675 cm^{-1} and 516.12 cm^{-1} belong to C–S stretching and CuS bonding, respectively [20, 50].

3.6 Optical studies

The optical absorption spectra of the CuS nanostructures (Fig. 10) synthesized by varying reaction times were recorded in the wavelength range of 300–800 nm. The optical absorption in the ultra-violet region is much higher than in the visible region where it has a steady rate. It has been reported that CuS nanoparticles have a wide absorption
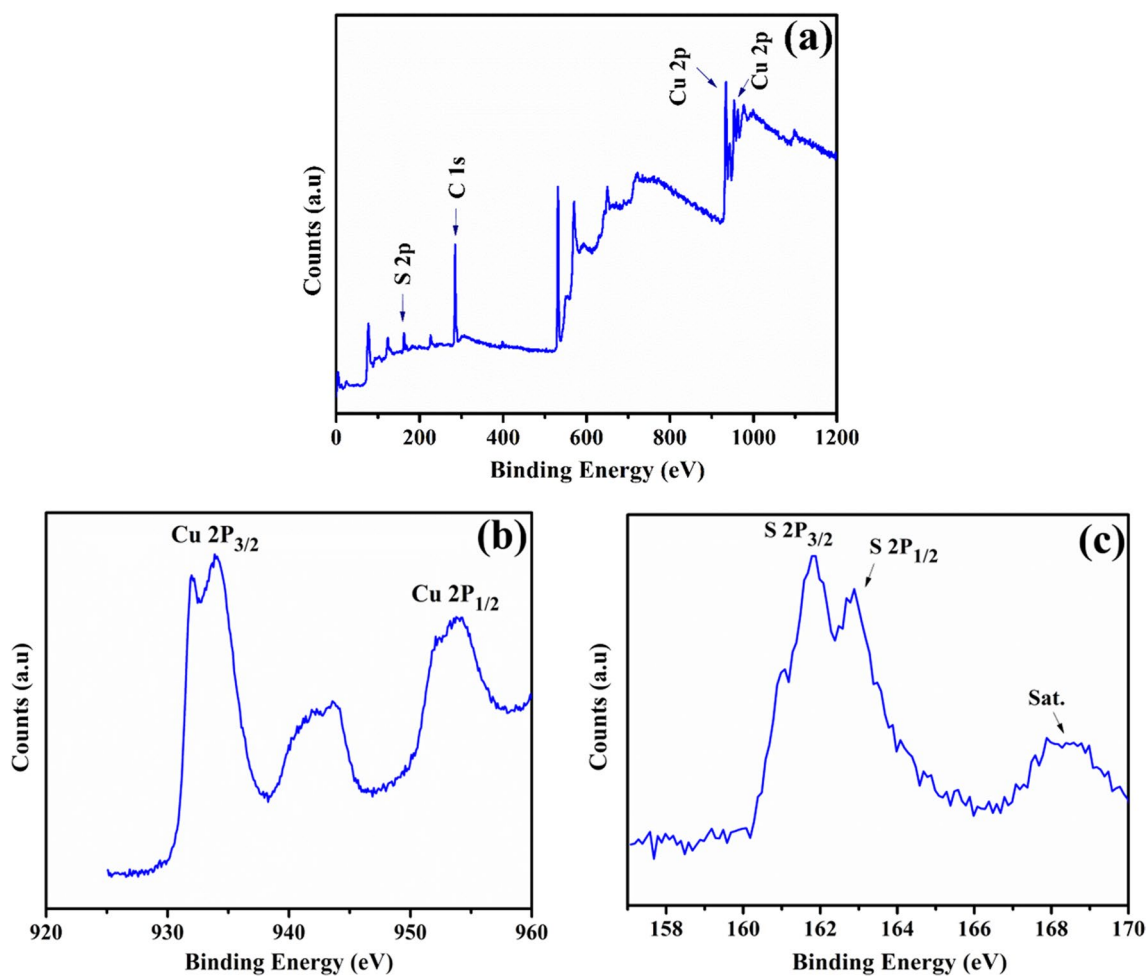
Fig. 7 XPS spectra for **a** survey scan, **b** copper (Cu), **c** sulfur (S) for CuS nanostructures synthesized at a reaction time of 16 h
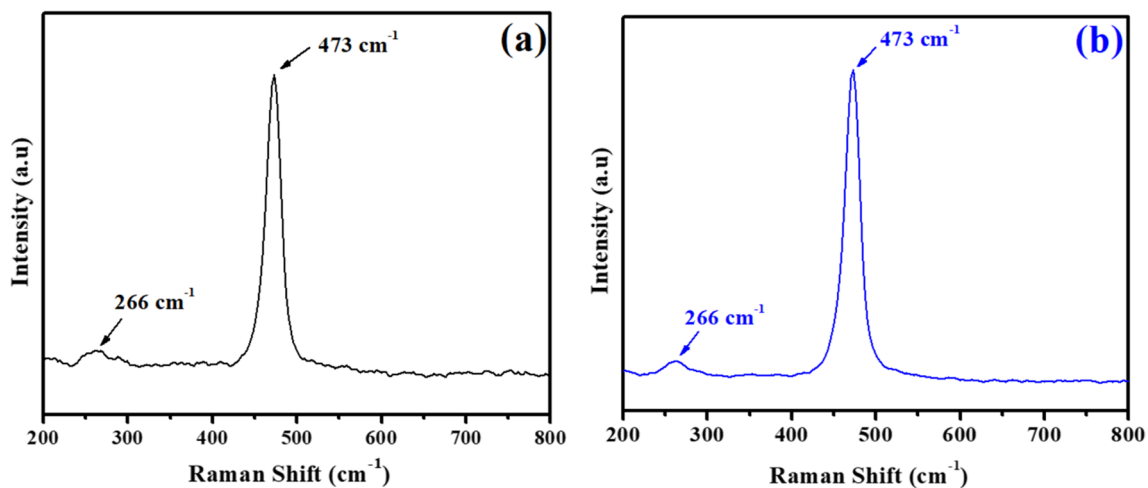

Fig. 8 Raman spectra for CuS nanostructures synthesized at a reaction time of **a** 8 h and **b** 16 h
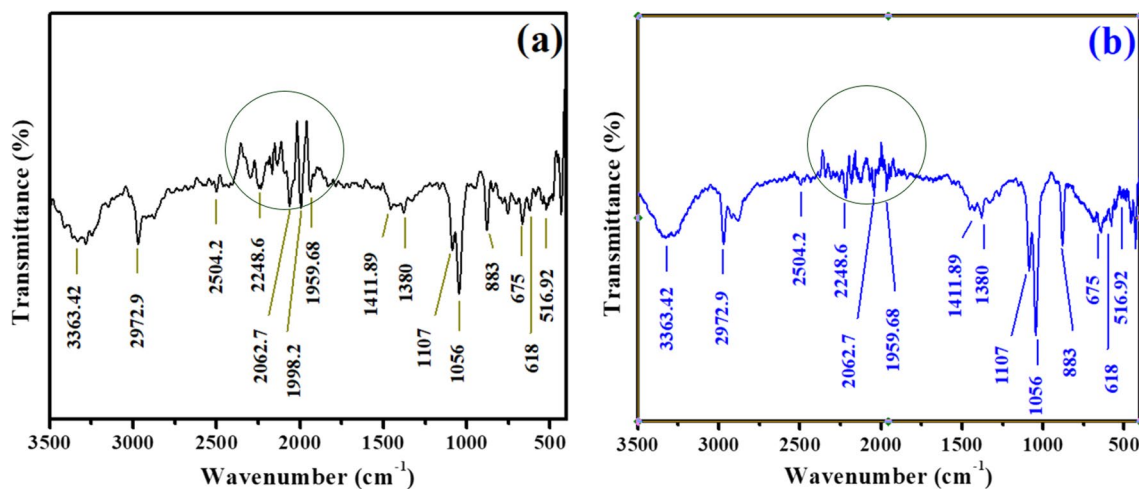
Fig. 9 FT-IR spectra for CuS nanostructures synthesized at reaction times of **a** 8 h and **b** 16 h
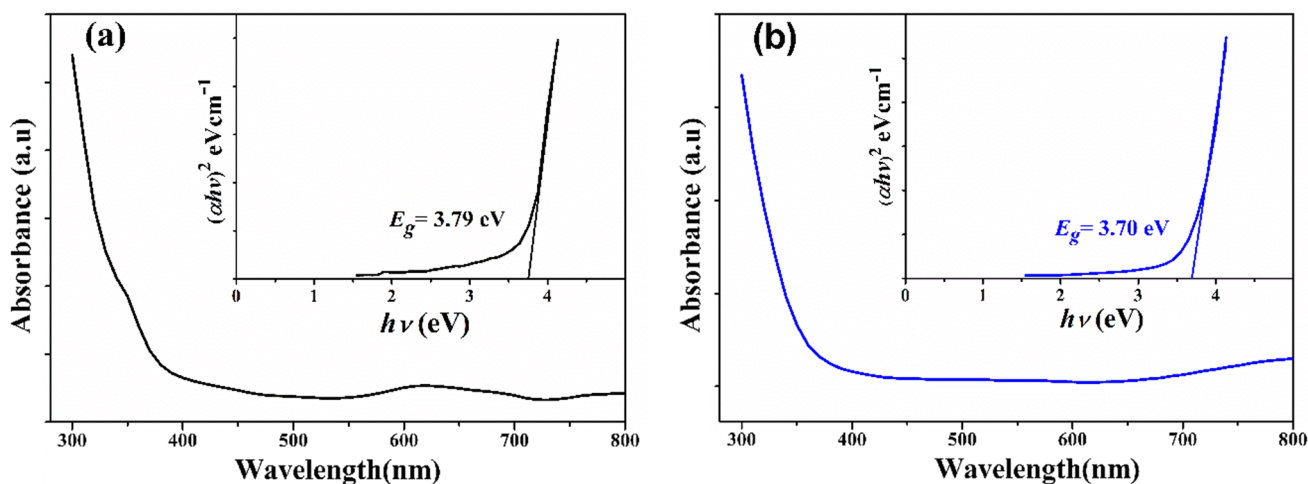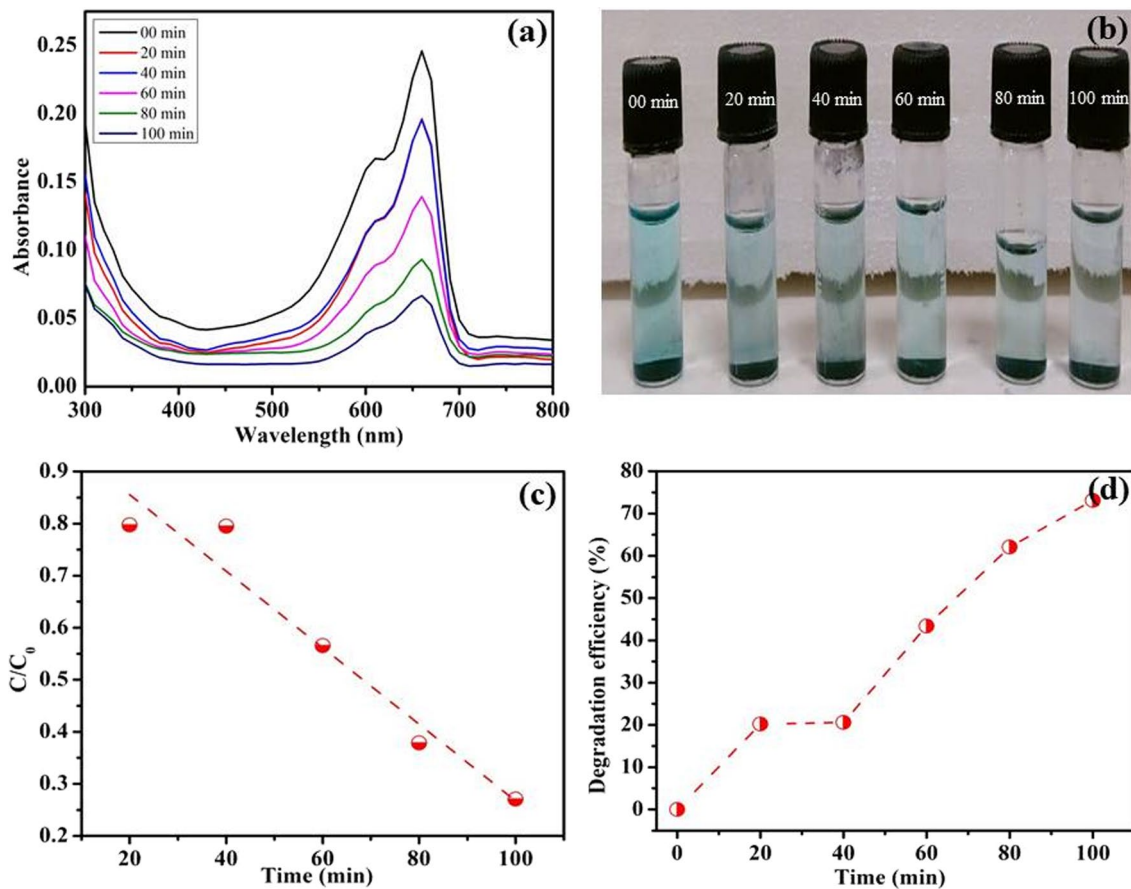

Fig. 10 Absorption spectra of CuS nanostructures synthesized at a reaction time of **a** 8 h and **b** 16 h with the inset depicting Tauc's plots

range as compared to bulk CuS [51]. The absorption edge of the synthesized nanostructures is observed to be slightly shifted toward the higher wavelength side with reaction time. The steepness of the absorption edge, Fig. 10a and b, is an indication of the direct bandgap nature of the CuS nanostructures. Optical bandgap energy (E_g) of the synthesized nanostructures at different reaction times, inset of Fig. 10a and b, was estimated using Tauc's plot i.e., $(\alpha h\nu)^2$ vs $h\nu$ from the absorption spectra [52]. Here α, h, and ν are the absorption coefficient, Planck's constant, and frequency of incident light, respectively. The estimated values for E_g are 3.79 eV and 3.70 eV for CuS nanostructures synthesized at reaction times 8 h and 16 h, respectively, and are in good agreement with reported values [51, 53]. However, slightly higher E_g values of the synthesized CuS nanostructures in comparison to the bulk CuS having $E_g = 2.5$ eV is attributed to the prevailing quantum size effect in the semiconductor

nanoparticles. The range of bandgap energy of the synthesized nanostructures may be suitable for the visible solar light-driven dye degradation purpose.

3.7 Photocatalytic activity

The photocatalytic behavior of the synthesized CuS nanostructures against organic water contaminants, methylene blue, and crystal violet dyes, under exposure to natural sunlight is examined. The optical absorbance spectra of aqueous MB solution (with initial concentration 2×10^{-5} M and volume 25 mL) in contact with CuS photocatalysts that tested at different time intervals are shown in Figs. 11a and 12a. The single peak observed at wavelength 663 nm in both spectra corresponds to the characteristic absorption peak for MB dye [54]. The intensity of this peak has been observed to decrease swiftly with increasing irradiation time which

Fig. 11 **a** Time-dependent UV–visible absorption spectra for the photodegradation of MB, **b** decoloration of MB as a function of time, **c** degree of degradation and **d** the degradation efficiency in the presence of CuS nanostructures synthesized at reaction time 8 h

directly indicates the degradation of the dye. Initially, there is a significant decrease in the concentration of MB dye in the presence of CuS photocatalyst under illumination till 60 min of exposure time for both samples. However, this decrease slowdown subsequently, and absorption has been observed to be negligible for CuS photocatalysts synthesized at 16 h. Further, it is clear that the intense bluish color of the starting MB solution containing CuS photocatalyst (from Figs. 11b and 12b) gradually fades with increasing natural light exposure time. The degree of photocatalytic dye degradation (C/C_0) as a function of time (Figs. 11c and 12c) has been estimated for each photodegradation w.r.t the maximum absorbance at 663 nm, where C_0 is the initial dye concentration and C is the concentration at reaction time t. It has been noticed that the CuS catalyst synthesized at 16 h has higher photocatalytic activity (with a rate constant of 0.61×10^{-2} min^{-1}) than the sample prepared at 8 h (with a rate constant of 0.73×10^{-2} min^{-1}) in the photodegradation of MB. The degradation efficiency of CuS photocatalysts prepared at 8 h and 16 for MB after 100 min exposure time (Figs. 11d and 12d) is found to be 73% and 76%, respectively.

Likewise, the absorbance spectra of aqueous CV solution (initial concentration 2×10^{-2} M, and volume 25 mL) comprising CuS photocatalyst dose have been tested at different exposure times (Figs. 13a and 14a). The single peak obtained at wavelength 592 nm resembles the characteristic absorption peak of CV dye [55]. The intensity of this peak has been observed to decrease more rapidly with increasing irradiation time for CV solution containing CuS catalyst prepared at 8 h than the catalyst prepared at 16 h. Both the samples indicate the degradation of CV dye in the presence of CuS photocatalyst and the absorption peak completely disappeared after about 100 min for the CV solution with CuS catalysts prepared at 8 h. As no new peak appears during the reaction, hence, degradation has been found successful within 100 min. This degradation is also supported by the gradual decoloration of the violet solution to transparent with increasing exposure time (Figs. 13b and 14b). Future, it has been analyzed that the CuS catalyst synthesized at 8 h exhibits higher photocatalytic activity (with a rate constant of 0.41×10^{-2} min^{-1}) than the sample prepared at 16 h (with a rate constant of 0.70×10^{-2} min^{-1}) in the degradation of CV dye (Figs. 13c and 14c). The degradation efficiency of
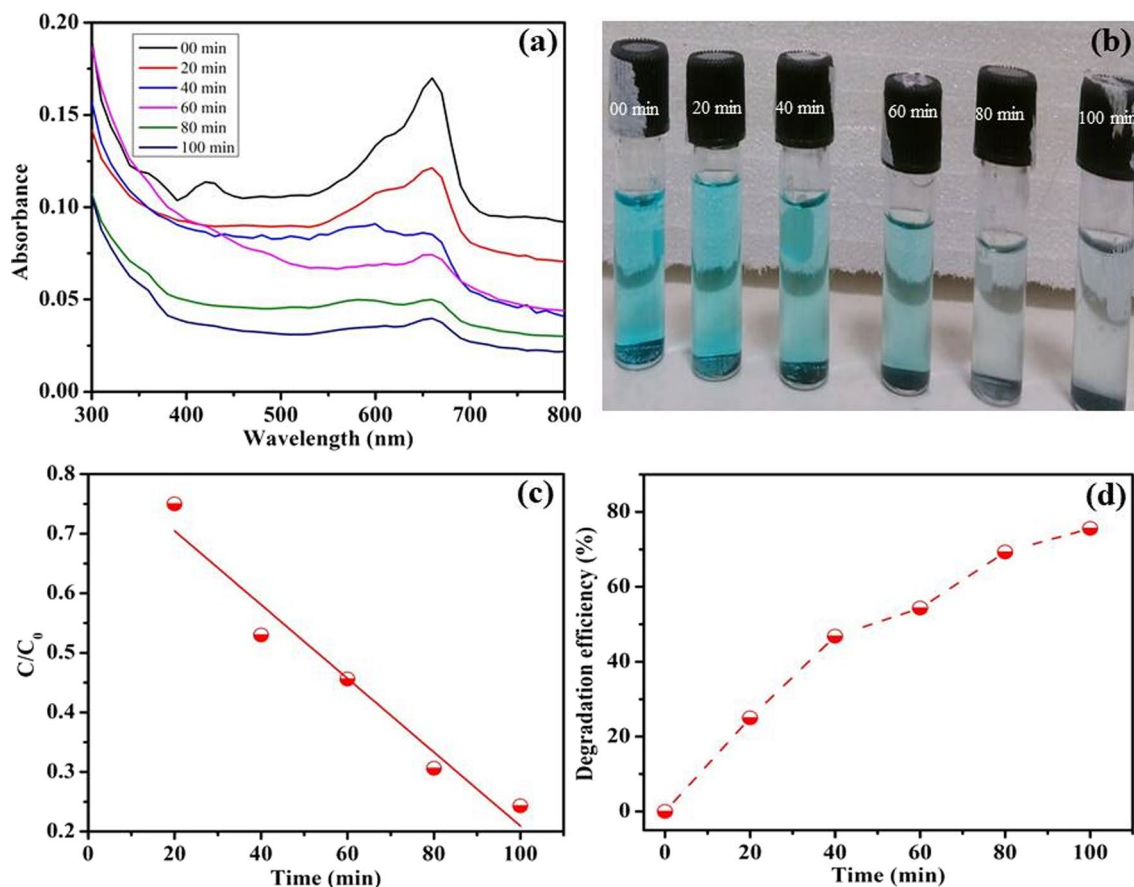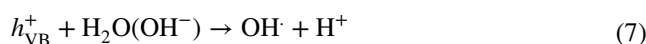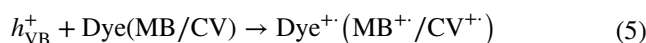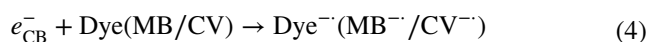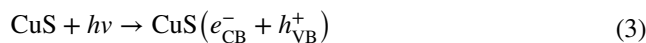
Fig. 12 **a** Time-dependent UV–visible absorption spectra for the photodegradation of MB, **b** decoloration of MB as a function of time, **c** degree of degradation and **d** the degradation efficiency in the presence of CuS nanostructures synthesized at reaction time 16 h
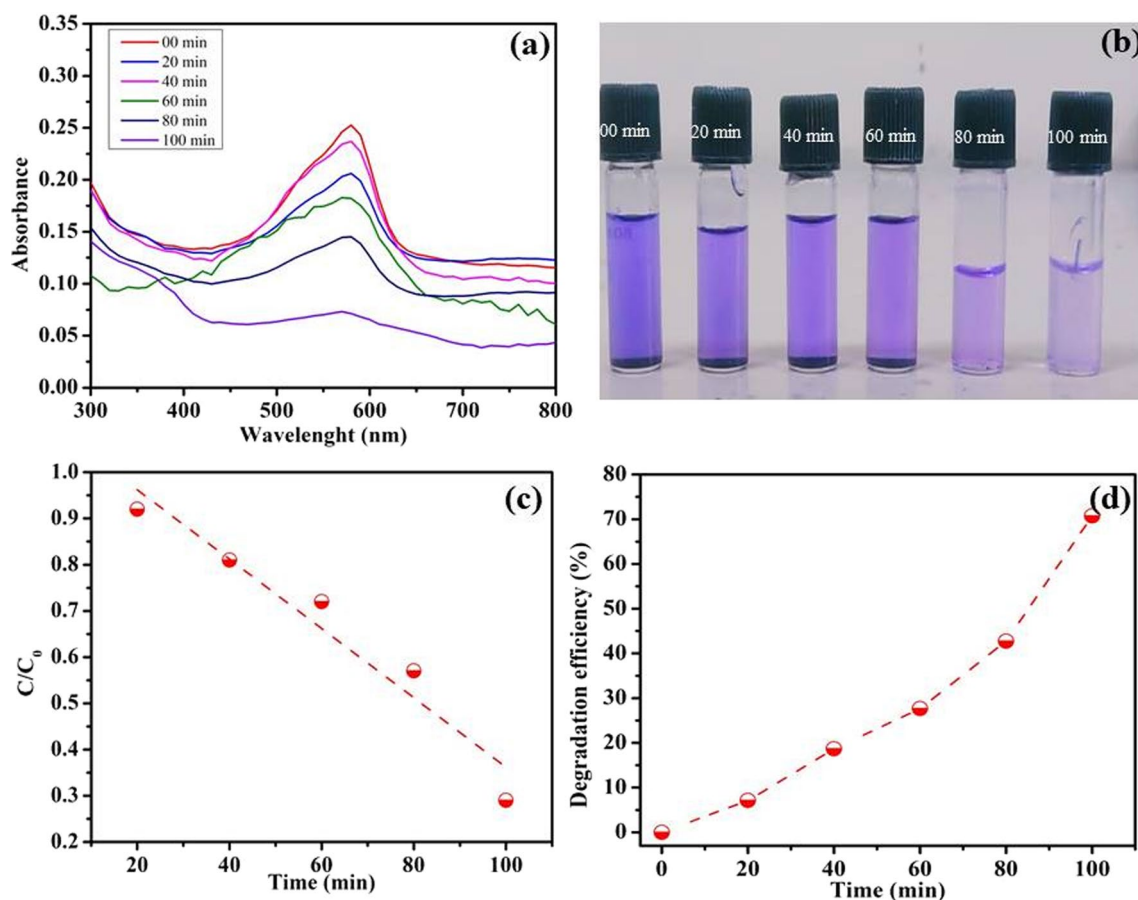
CuS photocatalysts, prepared at 8 h and 16 for CV, at the same exposure time (Figs. 13d and 14d) is found to be 72% and 65%, respectively.

3.8 Mechanism for dye degradation

Semiconductors in different nanostructures have excellent possibilities for applications in photocatalysis due to their distinct physical and chemical properties. The process of degradation is preceded basically in three steps, i.e., photon-induced excitation of charge carriers, separation of charges which is done by surface oxidation, and reduction process. It has been reported that semiconductors can absorb sunlight to catalyze different photochemical reactions and reactive oxygen species (ROS) which are the main intermediates in photocatalysis [56, 57]. The mechanism of degradation of organic dyes (MB and CV) supported by ROS generation under visible light is shown in Fig. 15. In all photocatalytic activities, the photons of energy equal to or greater than the bandgap of the catalyst get absorbed, and h^+, OH·, and $O_2^{-\cdot}$ radicals are the sources of ROS generation. These absorbed photons further generate photo-emitted electron–hole pairs

in the valance band and conduction band i.e., holes (h^+) in VB and electron (e^-) in CB. In the conduction band, the generated electrons (e^-) act as reducing agents which are captured oxygen molecules present on the surface of CuS nanostructures which further creates superoxide radicals. The function of the oxidizing agent is performed by holes (h^+) which are generated in the valence band and produce hydroxyl radicals by reacting with water. The proposed reaction mechanism for the degradation of organic dyes (MB and CV) is expressed by the following equations:

$$\text{CuS} + h\nu \rightarrow \text{CuS}\left(e_{\text{CB}}^- + h_{\text{VB}}^+\right) \tag{3}$$

$$e_{\text{CB}}^- + \text{Dye(MB/CV)} \rightarrow \text{Dye}^-(\text{MB}^-\cdot/\text{CV}^-\cdot) \tag{4}$$

$$h_{\text{VB}}^+ + \text{Dye(MB/CV)} \rightarrow \text{Dye}^{+\cdot}\left(\text{MB}^{+\cdot}/\text{CV}^{+\cdot}\right) \tag{5}$$

$$e_{\text{CB}}^- + O_{2(\text{aq})} \rightarrow O_2^{-\cdot} \tag{6}$$

$$h_{\text{VB}}^+ + \text{H}_2\text{O(OH}^-) \rightarrow \text{OH}^\cdot + \text{H}^+ \tag{7}$$

Fig. 13 **a** Time-dependent UV–visible absorption spectra for the photodegradation of CV, **b** decoloration of CV as a function of time, **c** degree of degradation and **d** the degradation efficiency in the presence of CuS nanostructures synthesized at reaction time 8 h

$$OH^. + O_2^{-.} + dye(MB/CV) \rightarrow DegradationProducts(CO_2 + H_2O) \quad (8)$$
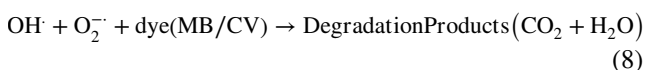
The photo-generated (h^+) holes in this process have a very limited direct role in photodegradation. In the whole degradation process, it is noticed that the addition of catalyst did not proceed to any degradation reaction alone. However, the presence of visible light is also an important factor for the reaction to proceed. The experimental results of the present study demonstrate that CuS nanostructures possess excellent photocatalytic behavior for MB and CV organic dyes, indicating its feasibility as a promising photocatalytic material for the degradation of organic pollutants.

The synthesized CuS structures have a great ability to degrade MB and CV dyes and they exhibit high photocatalytic activity (Table 2). Therefore, rose flower-shaped CuS structures are promising photocatalysts for water remediation in the visible-light region.

4 Conclusion

This work demonstrated the photocatalytic behavior of rose flower-shaped CuS nanostructures synthesized by solvothermal technique for different reaction times of 8 h and 16 h. The structural, morphological, compositional, and optical properties of synthesized nanostructures were observed using different characterization tools. The structural study revealed that the obtained nanostructures grow in hexagonal CuS geerite phase, polycrystalline in nature, and comprise crystallites having average sizes of 14.13 nm and 17.25 nm. The surface morphology disclosed rose flower-shaped nanostructures built by self-assembled nanoflakes in a hexagonal pattern. FE-SEM and TEM studies showed that the changing reaction time significantly influences the morphology of the nanostructures. The appearance of the elemental peaks as observed from EDS and XPS spectra confirms the presence of desired
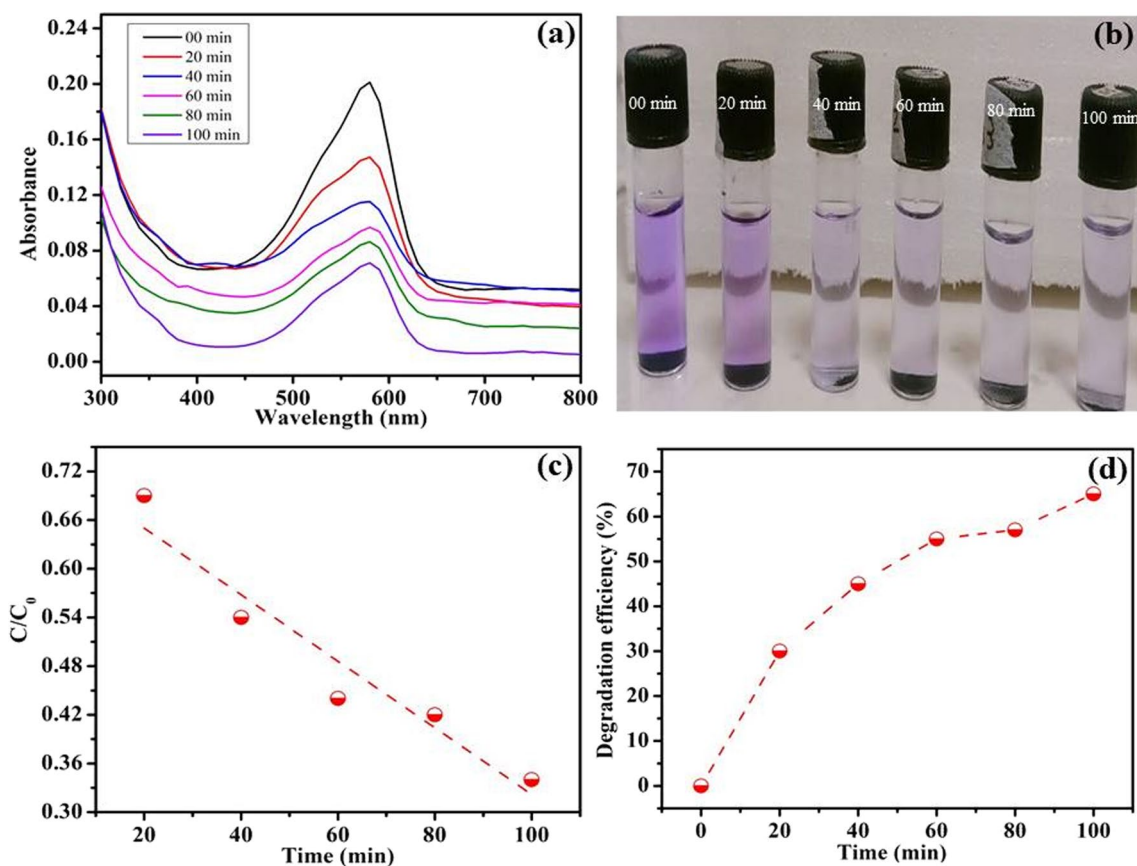
Fig. 14 **a** Time-dependent UV–visible absorption spectra for the photodegradation of CV, **b** decoloration of CV as a function of time, **c** degree of degradation and **d** the degradation efficiency in the presence of CuS nanostructures synthesized at reaction time 16 h

Fig. 15 Possible mechanism for the photodegradation of the organic dye
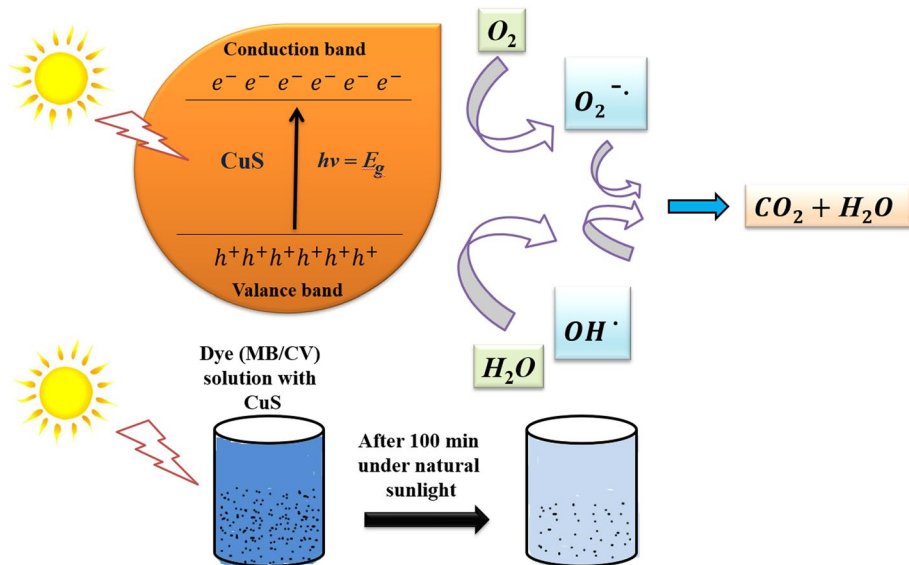
CuS material, while the absence of extra peaks confirms its purity. The optical studies showed broad absorption spectra of CuS nanoparticles in the visible range and the optical band gap value was found to decrease with reaction time. The photocatalytic activity of the synthesized CuS nanostructures was examined over MB and CV organic

Table 2 Comparison of photocatalytic activity of different CuS structures for the degradation of different organic dyes

Photocatalyst system	Synthesis method	Dosage (g/L)	Targeted dye	Concentration of dye	Energy type	Degradation (%)	Time (min)	References
CuS flower-micro-spheres	Elemental direct reaction	0.1	$MB + H_2O_2$	10 mg/L	Visible light	94.20	45	[4]
CuS nanoflow-ers	Rapid polyol facile route	0.3	RhB	5×10^{-6} mol/L	Visible light	90.00	60	[7]
CuS hexagon flakes-like structure	Solvothermal	1.0	$RhB + H_2O_2$	20 mg/L	Visible light	99.70	60	[14]
CuS nanotubes	Radiolytic	1.0	$RhB + H_2O_2$	1×10^{-4} mol/L	Visible light	70.00	100	[16]
CuS micro-spheres	Solvothermal	0.02	$MB + H_2O_2$	400 mg/L	Natural light	93.00	48	[19]
CuS rose-like microsphere	Solvothermal	0.01	$RhB + H_2O_2$	10 mg/L	Visible light	99.00	8	[24]
			$MB + H_2O_2$			99.00	10	
			$MO + H_2O_2$			97.00	10	
CuS nanopar-ticles	Solvothermal	0.03	MB	2×10^{-5} M, 50 mL	Solar light	85.13	240	[26]
					Visible light	90.29		
					UV light	85.13		
			RB	2×10^{-5} M, 50 mL	Solar light	69.23		
					Visible light	60.37		
					UV light	50.04		
			EV	2×10^{-5} M, 50 mL	Solar light	91.97		
					Visible light	56.02		
					UV light	79.49		
			CR	2×10^{-5} M, 50 mL	Solar light	60.35		
					Visible light	63.21		
					UV light	75.47		
CuS nanopar-ticles	Hydrothermal	0.05	$MB + K_2Cr_2O_7$	1.25×10^{-5} M	Visible light	95	30	[37]
CuS ball flower	Hydrothermal	1.0	$RhB + H_2O_2$	2×10^{-5} M, 50 mL	UV light	99	60	[53]
CuS rose flower-shape	Solvothermal	0.02	MB	2×10^{-5} M, 25 mL	Natural light	76	100	This work
CuS rose flower-shape	Solvothermal	0.02	CV	2×10^{-5} M, 25 mL	Natural light	72	100	

dyes under natural sunlight exposure for the time duration of 100 min. The degradation efficiency of 76% and 73% for the MB dye was achieved by 0.5 mg dose of CuS photocatalysts prepared at 8 h and 16 h, respectively. Moreover, the efficiency was 72% and 65% for the CV dye by the same photocatalysts prepared at 8 h and 16 h, respectively. Finally, it can be expected that the possibility of using rose flower-shaped CuS nanostructures for the degradation of organic dyes, especially MB and CV, in natural sunlight is appreciable and helpful in the remediation of water pollution.

Declarations

References

1. M. Dibyananda, Y.P. Bhoi, P.K. Samal, B.G. Mishra, Morphology controlled synthesis and photocatalytic study of novel

CuS-Bi$_2$O$_2$CO$_3$ heterojunction system for chlorpyrifos degradation under visible light illumination. Appl. Surf. Sci. **455**, 891–902 (2018). https://doi.org/10.1016/j.apsusc.2018.06.051

2. P.O. Oladoye, T.O. Ajiboye, E.O. Omotola, O.J. Oyewola, Methylene blue dye: toxicity and potential elimination technology from wastewater. Res. Eng. **16**, 1230–2590 (2022). https://doi.org/10.1016/j.rineng.2022.100678

3. N. Salahudeen, A.A. Rasheed, Kinetics and thermodynamics of hydrolysis of crystal violet at ambient and below ambient temperatures. Sci. Rep. **10**(1), 1–9 (2020). https://doi.org/10.1038/s41598-020-78937-4

4. L. Song, Y. Zeng, Y. Cheng, G. Luo, Synthesis of CuS microspheres from constituent elements and its photocatalytic application. Mater. Res. Innov. **21**(4), 232–236 (2017). https://doi.org/10.1080/14328917.2016.1207043

5. X. Wang, K. Maeda, A. Thomas, K. Takanabe, G. Xin, J.M. Carlsson, M. Antonietti, A metal-free polymeric photocatalyst for hydrogen production from water under visible light. Nat. Mater. **8**(1), 76–80 (2009). https://doi.org/10.1038/nmat2317

6. Z. Yi, J. Ye, N. Kikugawa, T. Kako, S. Ouyang, H.S. Williams, H. Yang, J. Cao, W. Luo, Z. Li, Y. Liu, R.L. Withers, An orthophosphate semiconductor with photooxidation properties under visible-light irradiation. Nat. Mater. **9**(7), 559–564 (2010). https://doi.org/10.1038/nmat2780

7. T.Y. Ding, M.S. Wang, S.P. Guo, G.C. Guo, J.S. Huang, CuS nanoflowers prepared by a polyol route and their photocatalytic property. Mater. Lett. **62**, 4529–4531 (2008). https://doi.org/10.1016/j.matlet.2008.08.031

8. J. Ma, Q. Du, H. Ge, Q. Zang, Fabrication of core-shell TiO$_2$@CuS nanocomposite via a bifunctional linker-assisted synthesis and its photocatalytic performance. J. Mater. Sci. **54**, 2928–2939 (2019). https://doi.org/10.1007/s10853-018-3054-1

9. M.M. Munoz, J.E.R. Ibarra, J.E.R. Paez, M.D. Teodoro, G.E. Marques, A.R. Sanabria, J.A.H. Coaquira, Role of defects on the enhancement of the photocatalytic response of ZnO nanostructures. Appl. Surf. Sci. **448**, 646–654 (2018). https://doi.org/10.1016/j.apsusc.2018.04.105

10. F. Fresno, R. Portela, S. Suarez, J.M. Coronado, Photocatalytic materials: recent achievements and near future trends. J. Mater. Chem. A **2**, 2863–2884 (2014). https://doi.org/10.1039/C3TA13793G

11. M. Kamranifar, A. Allahresani, A. Naghizadeh, Synthesis and characterizations of a novel CoFe$_2$O$_4$@CuS magnetic nanocomposite and investigation of its efficiency for photocatalytic degradation of penicillin G antibiotic in simulated wastewater. J. Hazard. Mater. **366**, 545–555 (2019). https://doi.org/10.1016/j.jhazmat.2018.12.046

12. K. Das, D. Majhi, Y.P. Bhoi, B.G. Mishra, Combustion synthesis, characterization and photocatalytic application of CuS/Bi4Ti$_3$O$_{12}$ *p-n* heterojunction materials towards efficient degradation of 2-methyl-4-chlorophenoxyacetic acid herbicide under visible light. Chem. Eng. J. **362**, 588–599 (2019). https://doi.org/10.1016/j.cej.2019.01.060

13. P. Roy, S.K. Srivastava, Nanostructured copper sulfides: synthesis, properties and applications. CrystEngComm **17**(41), 7801–7815 (2015). https://doi.org/10.1039/c5ce01304f

14. M. Wang, F. Xie, W. Li, M. Chen, Y. Zhao, Preparation of various kinds of copper sulfides in a facile way and the enhanced catalytic activity by visible light. J. Mater. Chem. A **1**(30), 8616–8621 (2013). https://doi.org/10.1039/c3ta11739a

15. N.F. Khairol, N. Sapawe, Electrosynthesis of ZnO nanoparticles deposited onto eggshell for degradation of Congo red. Mater. Today Proc. **5**(10), 21936–21939 (2018). https://doi.org/10.1016/j.matpr.2018.07.053

16. Z. Hai, J. Huang, H. Remita, J. Chen, Radiolytic synthesis of CuS nanotubes with photocatalytic activity under visible light. Mater. Lett. **108**, 304–307 (2013). https://doi.org/10.1016/j.matlet.2013.07.027

17. L. Isac, C. Cazan, A. Enesca, L. Andronic, Copper sulfide-based heterojunctions as photocatalysts for dyes photodegradation. Front. Chem. **7**, 1–9 (2019). https://doi.org/10.3389/fchem.2019.00694

18. R. Zeinodin, F.J. Sheini, In-doped CuS nanostructures: Ultrasonic synthesis, physical properties, and enhanced photocatalytic behavior. Phys. B Condens. Matter **570**, 148–156 (2019). https://doi.org/10.1016/j.physb.2019.05.048

19. M. Tanveer, C. Cao, Z. Ali, I. Aslam, F. Idrees, W.S. Khan, N. Mahmood, Template-free synthesis of CuS nanosheet-based hierarchical microspheres: an efficient natural light driven photocatalyst. CrystEngComm **16**(24), 5290–5300 (2014). https://doi.org/10.1039/c4ce00090k

20. S. Iqbal, A. Bahadur, S. Anwer, S. Ali, R.M. Irfan, H. Li, M. Shoaib, M. Raheel, T. Ali Anjum, M. Zulqarnain, Effect of temperature and reaction time on the morphology of L-cysteine surface capped chalcocite (Cu$_2$S) snowflakes dendrites nanoleaves and photodegradation study of methyl orange dye under visible light. Colloids Surf A Physicochem. Eng. Asp. **601**, 124984 (2020). https://doi.org/10.1016/j.colsurfa.2020.124984

21. V. Dhiman, S. Kumar, M. Kaur, R. Sharma, T. Chandel, D. Bhardwaj, D. Prasher, Synergistic effect of stirring and marigold shaped Cu$_2$FeSnS$_4$ nanostructure for the enhanced performance of Rhodamine B degradation under visible light. Inorg. Chem. Commun. **154**, 110923 (2023). https://doi.org/10.1016/j.inoche.2023.110923

22. X. Cao, H. Zeng, M. Wang, X. Xu, M. Fang, S. Ji, L. Zhang, Large scale fabrication of quasi-aligned ZnO stacking nanoplates. J. Phys. Chem. C **112**(14), 5267–5270 (2008). https://doi.org/10.1021/jp800499r

23. N. Zheng, X. Bu, P. Feng, Open-framework chalcogenides as visible-light photocatalysts for hydrogen generation from water. Angew. Chem. - Int. Ed. **44**(33), 5299–5303 (2005). https://doi.org/10.1002/anie.200500346

24. L. Zhao, L. Zhou, C. Sun, Y. Gu, W. Wen, X. Fang, Rose-like CuS microflowers and their enhanced visible-light photocatalytic performance. CrystEngComm **20**(41), 6529–6537 (2018). https://doi.org/10.1039/c8ce00888d

25. B. Zhang, X.W. Gao, J.Z. Wang, S.L. Chou, K. Konstantinov, H.K. Liu, CuS nanoflakes, microspheres, microflowers, and nanowires: synthesis and lithium storage properties. J. Nanosci. Nanotechnol. **13**(2), 1309–1316 (2013). https://doi.org/10.1166/jnn.2013.5987

26. D. Ayodhya, M. Venkatesham, A. Santoshi, Photocatalytic degradation of dye pollutants under solar, visible and UV lights using green synthesised CuS nanoparticles. J. Exp. Nanosci. **11**(6), 418–432 (2015). https://doi.org/10.1080/17458080.2015.1070312

27. J. Fang, P. Zhang, H. Chang, X. Wang, Hydrothermal synthesis of nanostructured CuS for broadband efficient optical absorption and high-performance photo-thermal conversion. Sol. Energy Mater. Sol. Cells **185**, 456–463 (2018). https://doi.org/10.1016/j.solmat.2018.05.060

28. S. Kumar, J.K. Sharma, Stable phase CdS nanoparticles for optoelectronics: a study on surface morphology, structural and optical characterization. Mater. Sci. Pol. **34**(2), 368–373 (2016). https://doi.org/10.1515/msp-2016-0033

29. Y. Gu, T. Li, Y. Jiang, W. Wen, J. Wu, L. Zhao, Copper sulfide nanostructures and their sodium storage properties. CrystEngComm **22**, 7082–7089 (2020). https://doi.org/10.1039/d0ce01059f

30. P. Vinothkumar, C. Manoharan, B. Shanmugapriya, M. Bououdina, Effect of reaction time on structural, morphological, optical and photocatalytic properties of copper oxide (CuO) nanostructures. J. Mater. Sci. Mater. Electron. **30**(6), 6249–6262 (2019). https://doi.org/10.1007/s10854-019-00928-7

31. G.C. Collazzo, S.L. Jahn, N.L.V. Carreño, E.L. Foletto, Temperature and reaction time effects on the structural properties of titanium dioxide nanopowders obtained via the hydrothermal method. Braz. J. Chem. Eng. **28**(2), 265–272 (2011). https://doi.org/10.1590/S0104-66322011000200011

32. Z. Ajji, Grafting of poly (vinyl pyrrolidone) with citric acid using gamma irradiation. Nucl. Instrum. Methods Phys. Res., Sect. B **265**(1), 179–182 (2007). https://doi.org/10.1016/j.nimb.2007.08.087

33. C. Wang, E. Shen, E. Wang, L. Gao, Z. Kang, C. Tian, C. Zhang, Controllable synthesis of ZnO nanocrystals via a surfactant-assisted alcohol thermal process at a low temperature. Mater. Lett. **59**(23), 2867–2871 (2005). https://doi.org/10.1016/j.matlet.2005.04.031

34. N. Shanmugam, S. Cholan, N. Kannadasan, K. Sathishkumar, G. Viruthagiri, Effect of polyvinylpyrrolidone as capping agent on Ce^{3+} doped flowerlike ZnS nanostructure. Solid State Sci. **28**, 55–60 (2014). https://doi.org/10.1016/j.solidstatesciences.2013.12.008

35. Z. Cheng, S. Wang, Q. Wang, B. Geng, A facile solution chemical route to self-assembly of CuS ball-flowers and their application as an efficient photocatalyst. CrystEngComm **12**(1), 144–149 (2010). https://doi.org/10.1039/b914902c

36. Y. Zhang, B. Zhang, Z. Ge, L. Zhu, Y. Li, Preparation by solvothermal synthesis growth mechanism and photocatalytic performance of CuS. Eur. J. Inorg. Chem. **14**, 2368–2375 (2014). https://doi.org/10.1002/ejic.201400098

37. S. Agarwal, P. Phukan, D. Sarma, K. Deori, Versatile precursor-dependent copper sulfide nanoparticles as a multifunctional catalyst for the photocatalytic removal of water pollutants and the synthesis of aromatic aldehydes and NH-triazoles. Nanoscale Adv. **18**(13), 3954–3966 (2021). https://doi.org/10.1039/d1na00239b

38. M.M. Melake, J. Anqi, W. Gang, D.K. Macharia, G. Shanyi, X. Hongyao, Structure-based optical properties and catalytic activities of hydrothermally prepared CuS nanostructures. Nanotechnology **10**(30), 1–23 (2019). https://doi.org/10.1088/1361-6528/aaf758

39. A. Kale, Y. Bao, Z. Zhou, P.E. Prevelige, A. Gupta, Directed self-assembly of CdS quantum dots on bacteriophage P22 coat protein templates. Nanotechnology **24**(4), 045603 (2013). https://doi.org/10.1088/0957-4484/24/4/045603

40. B.M. Palve, S.R. Jadkar, H.M. Pathan, A simple chemical route to synthesis the CuS nanocrystal powder at room temperature and phase transition. J. Mater. Sci. Mater. Electron. **27**(11), 11783–11789 (2016). https://doi.org/10.1007/s10854-016-5318-3

41. A.K. Zardkhoshoui, S.S.H. Davarani, Construction of complex copper-cobalt selenide hollow structures as an attractive battery-type electrode material for hybrid supercapacitors. Chem. Eng. J. **402**, 126241 (2020). https://doi.org/10.1016/j.cej.2020.126241

42. A.K. Zardkhoshoui, B. Ameri, S.S.H. Davarani, A hybrid supercapacitor assembled by reduced graphene oxide encapsulated lollipop-like $FeNi_2S_4@Co_9S_8$ nanoarrays. Chem. Eng. J. **470**, 144132–144132 (2023). https://doi.org/10.1016/j.cej.2023.144132

43. B. Ameri, A.K. Zardkhoshoui, S.S.H. Davarani, Engineering raspberry-like $CuCo_2S_4@ZnS$ hollow particles encapsulated with reduced graphene oxide for hybrid supercapacitors. Mater. Chem. Front. **7**(15), 3127–3145 (2023). https://doi.org/10.1039/D3QM00212H

44. N.A. Yeryukov, A.G. Milekhin, L.L. Sveshnikova, T.A. Duda, L.D. Pokrovsky, A.K. Gutakovskii, D.R.T. Zahn, Synthesis and characterization of Cu_xS ($x = 1$–2) nanocrystals formed by the Langmuir–Blodgett technique. J. Phys. Chem. C **118**(40), 23409–23414 (2014). https://doi.org/10.1021/jp507355t

45. A.G. Milekhin, N.A. Yeryukov, L.L. Sveshnikova, T.A. Duda, E.E. Rodyakina, V.A. Gridchin, E.S. Sheremet, D.R.T. Zahn, Combination of surface and interference-enhanced Raman scattering by CuS nanocrystals on nanopatterned Au structures. Beilstein J. Nanotechnol. **6**, 749–754 (2015). https://doi.org/10.3762/bjnano.6.77

46. Y. Deng, A.D. Handoko, Y. Du, S. Xi, B.S. Yeo, In situ Raman spectroscopy of copper and copper oxide surfaces during electrochemical oxygen evolution reaction: identification of Cu^{III} oxides as catalytically active species. ACS Catal. **6**(4), 2473–2481 (2016). https://doi.org/10.1021/acscatal.6b00205

47. I. Savarimuthu, M.J.A.M. Susairaj, CuS nanoparticles trigger sulfite for fast degradation of organic dyes under dark conditions. ACS Omega **7**(5), 4140–4149 (2022). https://doi.org/10.1021/acsomega.1c05697

48. M.R. Hosseini, M. Schaffie, M. Pazouki, E. Darezereshki, M. Ranjbar, Biologically synthesized copper sulfide nanoparticles: production and characterization. Mater. Sci. Semicond. Process. **15**(2), 222–225 (2012). https://doi.org/10.1016/j.mssp.2012.03.012

49. S. Iqbal, N.A. Shaid, M.M. Sajid, Y. Javed, A. Mahmood, G. Ahmad, M. Sarwar, Extensive evaluation of changes in structural, chemical and thermal properties of copper sulfide nanoparticles at different calcination temperature. J. Cryst. Growth **547**, 125823 (2020). https://doi.org/10.1016/j.jcrysgro.2020.125823

50. M.T. Ramesan, Synthesis characterization and conductivity studies of polypyrrole copper sulfide nanocomposites. J. Appl. Polym. Sci. **3**(128), 1540–1546 (2012). https://doi.org/10.1002/app.38304

51. X. Yan, E. Michael, S. Komarneni, Microwave- and conventional-hydrothermal synthesis of CuS, SnS, and ZnS: Optical properties. Ceram. Int. **39**(5), 4757–4763 (2013). https://doi.org/10.1016/j.ceramint.2012.11.062

52. S. Kumar, P. Sharma, V. Sharma, Redshift in absorption edge of $Cd_{1-x}Co_xS$ nanofilms. IEEE Trans. Nanotechnol. **13**(2), 343–348 (2014). https://doi.org/10.1109/TNANO.2014.2303200

53. A. Dasari, V. Guttena, Facile fabrication, characterization and efficient photocatalytic activity of surfactant-free ZnS, CdS and CuS nanoparticles. J. Sci.: Adv. Mater. Devices **4**(3), 381–391 (2019). https://doi.org/10.1016/j.jsamd.2019.08.006

54. J. Yao, C. Wang, Decolorization of methylene blue with TiO_2 sol via UV irradiation photocatalytic degradation. Int. J. Photoenergy **2010**, 1–6 (2010). https://doi.org/10.1155/2010/643182

55. S.P. Smrithi, N. Kottam, V. Arpitha, A. Narula, G.N.A. Kumar, K.R.V. Subramanian, Tungsten oxide modified with carbon nanodots: Integrating adsorptive and photocatalytic functionalities for water remediation. J. Sci.: Adv. Mater. Devices **5**(1), 73–83 (2020). https://doi.org/10.1016/j.jsamd.2020.02.005

56. X. Wang, L. So, R. Su, S. Wendt, P. Hald, A. Mamakhel, F. Besenbacher, The influence of crystallite size and crystallinity of anatase nanoparticles on the photo-degradation of phenol. J. Catal. **310**, 100–108 (2014). https://doi.org/10.1016/j.jcat.2013.04.022

57. S. Fizza, M.A. Rafiq, M.F. Afsar, M.M. Hasan, M.M. Chaudhry, Enhancement of degradation of mordant orange, safranin-O and acridine orange by CuS nanoparticles in the presence of H_2O_2 in dark and in ambient light. J. Mater. Sci. Mater. Electron. **29**, 19180–19191 (2018). https://doi.org/10.1007/s10854-018-0044-7

Authors and Affiliations

Vishal Dhiman[1] · Manmeet Kaur[1] · Dixit Prasher[1,2] · Deepesh Bhardwaj[3] · Kushvinder Kumar[4] · Suresh Kumar[1] ⬤

✉   Suresh Kumar
    sureshlakhanpal@gmail.com

[1]   Department of Physics, MM Engineering College, Maharishi
      Markandeshwar (Deemed to be University), Mullana,
      Ambala, Haryana 133207, India

[2]   Centre for Sustainable Materials Research and Technology,
      SMaRT@UNSW, School of Materials Science
      and Engineering, UNSW, Sydney, NSW 2052, Australia

[3]   Department of Chemistry, ITM Group of Institutions,
      Gwalior, MP 474002, India

[4]   Department of Chemistry, Panjab University,
      Chandigarh 160014, India